Geolocalization of Large-Scale DAS Channels Using a GPS-Tracked Moving Vehicle

Ettore Biondi^{*1}, Xin Wang², Ethan F. Williams¹, and Zhongwen Zhan¹

Abstract

Geolocalization of distributed acoustic sensing (DAS) array channels represents a crucial step whenever the technology is deployed in the field. Commonly, the geolocalization is performed using point-wise active-source experiments, known as tap tests, conducted in the vicinity of the recording fiber. However, these controlled-source experiments are time consuming and greatly diminish the ability to promptly deploy such systems, especially for large-scale DAS experiments. We present a geolocalization methodology for DAS instrumentation that relies on seismic signals generated by a geotracked vehicle. We demonstrate the efficacy of our workflow by geolocating the channels of two DAS systems recording data on dark fibers stretching approximately 100 km within the Long Valley caldera area in eastern California. Our procedure permits the prompt calibration of DAS channel locations for seismic-related applications such as seismic hazard assessment, urban-noise monitoring, wavespeed inversion, and earthquake engineering. We share the developed set of codes along with a tutorial guiding users through the entire mapping process.

Cite this article as Biondi, E., X. Wang, E. F. Williams, and Z. Zhan (2022). Geolocalization of Large-Scale DAS Channels Using a GPS-Tracked Moving Vehicle, *Seismol. Res. Lett.* **94**, 318–330, doi: 10.1785/0220220169.

Supplemental Material

Introduction

Seismological applications of distributed acoustic sensing (DAS) with dark fibers (i.e., pre-existing telecommunication cables) are growing remarkably in the last few years (Zhan, 2020; Biondi *et al.*, 2021). Multiple studies have demonstrated how DAS arrays are effective tools for accurately identifying shallow-surface structures and continuously monitoring urban noise (Martin and Biondi, 2018; Ajo-Franklin *et al.*, 2019; Lindsey *et al.*, 2019; Tribaldos *et al.*, 2021; Yang *et al.*, 2022). More recent DAS experiments showed the ability to record local and regional earthquakes along tens of kilometers of fiber (Li *et al.*, 2021; Nayak *et al.*, 2021). Thanks to DAS technology advances, the range of a single interrogator unit (IU) can now transform as much as 100 km of optical fiber into an ultradense seismic array (Karrenbach *et al.*, 2021).

When employing dark fibers for recording seismic data using DAS, the spatial locations of the array channels must be determined. One could utilize the fiber map provided by the fiber owner and the nominal channel spacing, usually set by the user as an acquisition parameter, to interpolate approximate channel locations. However, telecommunication cables typically include slack loops placed in manholes for maintenance. In addition, fiber layouts could present complicated geometries or suffer from inaccurate mapping. These complications prevent accurate interpolations, especially when the interrogator records data along tens of kilometers of fiber. For

this reason, a standard procedure in the field is to perform a tap test (Martin et al., 2017; Klaasen et al., 2021). This procedure consists of a series of controlled seismic sources (e.g., weight drops or a sledged hammer hitting a steel plate) conducted in the proximity of the recording fiber cable. Each point-wise source provides an accurate location of the closest excited DAS channel, which usually records the maximum amplitude. The major drawback of this approach is its cost and time inefficiency when applied to large-scale DAS arrays, where hundreds of sources are needed to accurately map the entire array.

Dark fibers are often located along other extended infrastructure, such as roads and highways. Such fibers, when transformed into a DAS array, can clearly detect vehicles moving in their proximity (Huot *et al.*, 2018; Liu *et al.*, 2018). Recently published studies described the ability to monitor vehicle traffic and characterize the near-surface properties using such vehicle-related signals (Wang *et al.*, 2020; Yuan *et al.*, 2020; Lindsey *et al.*, 2020). Because DAS can detect car-induced

^{1.} Seismological Laboratory, California Institute of Technology, Pasadena, California, U.S.A., https://orcid.org/0000-0002-3305-0982 (EB); https://orcid.org/0000-0002-6471-4497 (EFW); https://orcid.org/0000-0002-5586-2607 (ZZ); 2. Institute of Geology and Geophysics, Chinese Academy of Sciences, Beijing, Peoples's Republic of China

^{*}Corresponding author: ebiondi@caltech.edu

[©] Seismological Society of America

deformations, we can avoid using point-wise controlled sources to locate DAS channels and instead employ a geotracked moving vehicle generating seismic energy and quasistatic deformations along the recording cable (i.e., strain signals that do not present a wave-like or propagation behavior). The vehicle's position is tracked using a global positioning system (GPS) device and the recording DAS clock is GPS synchronized. The vehicle locations are then used to accurately locate the closest channels excited by the moving car. Yuan et al. (2021) described a similar process applied to a small-scale DAS array by leveraging the constant-speed drives of a GPStracked vehicle. Our study extends the application of this idea to large-scale arrays presenting complex fiber geometries. Our methodology dramatically diminishes the time and cost of any point-wise tap-test field experiment. We first describe our vehicle-based tap-test method, and then demonstrate its usage in locating the channels of two DAS arrays recording data in the Long Valley caldera area in eastern California, whose combined range reaches almost 100 km. Finally, because our workflow is based on interactive interfaces, we include the implemented software and a short tutorial describing the code usage.

Methodology

The overall workflow of our vehicle-based workflow can be divided into three main steps:

- create a vehicle location-time curve.
- process strain records and remove channels belonging to fiber loops, and
- calibrate the location-time curve against processed strain records.

The first two steps are independent from one another, whereas the final calibration must be performed after completing the previous ones (Fig. 1).

We start by projecting the vehicle locations onto the closest fiber latitude and longitude points. The fiber map is usually obtained from the owning telecommunication company. The provided fiber map is assumed to be precise (i.e., to allow the clear identification of the geotracked-vehicle signal), and our process enables the accurate positioning of the DAS array channels. To each fiber location we assign a relative distance with respect to the IU position. This function represents the piece-wise distance along the curved fiber and not geographical position from the reference point. With this process, we can define a curve that is the vehicle position along the fiber as a function of time.

The strain recordings represent the other necessary input of the workflow. We apply a band-pass filter between 0.5 and 15 Hz to the recordings and use them to identify and remove fiber slack loops, usually located in correspondence with maintenance manholes. DAS channels located within fiber loops

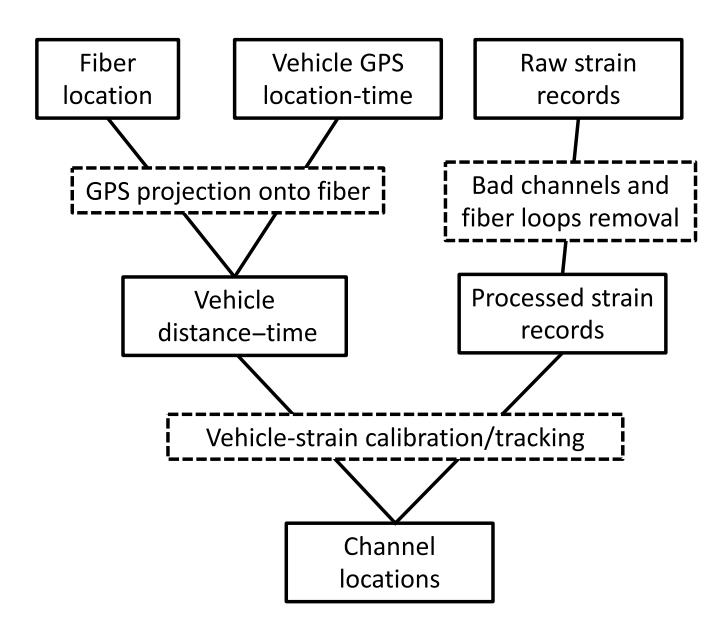


Figure 1. Vehicle-based tap-test workflow schematic describing the necessary steps to locate distributed acoustic sensing (DAS) channels. The solid-frame boxes represent the inputs and outputs of the calibration steps indicated by the dashed-frame boxes.

exhibit poor coupling and hence cannot provide any useful strain measurements. In addition, depending on the dark fiber properties (i.e., optical scattering properties and coupling), some DAS channels may show unusable high or low amplitudes and should be ignored during further analysis as well. An initial estimate of these uninformative channels can be done by computing the following quality factor *Q* for each channel:

$$Q(ch) = |E(ch) - \mu_E|/\sigma_E, \tag{1}$$

in which μ_E and σ_E are the mean and standard deviation of the signal's energy computed across all the channels within the strain recordings, respectively, and E represents the energy within a given channel ch (i.e., sum of squared amplitudes). Any channels having a Q-value above a certain threshold are considered anomalous. In our tests, we initially choose this threshold to be equal to 1.5 to help the initial identification of bad channels. Even though this process provides an initial guess for bad channels, we found that a visual inspection and selection must also be performed to identify these channels accurately. A higher value should be used in the presence of strong site effects or clipping effects due to the limitation of DAS dynamic-amplitude range. In the next section, we show an example of this process in which a local earthquake is used to remove bad channels from the DAS records. This removal process only needs to be performed once, because the indices of these uninformative channels do not change over time assuming a fixed channel-spacing parameter. Finally, to use the DAS data for the channel-localization process, we filter the recordings

to retain the frequency between 0.5 and 2.0 Hz, which is the band containing most of the quasi-static vehicle deformation.

Once the aforementioned steps are complete, we proceed to shift the vehicle's alongfiber distance curve to match the peak of the corresponding deformation quasi-static recorded in the DAS data. The first-order shifting, within approximately the duration of the signal (i.e., 1 s of the assumed tracked deformation), is performed manually. The final matching is done by automatically picking the maximum of the envelope of the strain within a 1 s window. This process allows us to select times for which our tracked car induced fiber deformations are recorded by the DAS system. Because the car's position for each time is known and has been projected onto the closest fiber location, we can assign this location to the channel in which the distance-time curve matches the corresponding vehicle-generated deformation. We perform

this procedure in a piece-wise fashion and calibrate only channels for all cable sections in which the tracked vehicle induced identifiable quasi-static signals, which limits the accumulation of errors from previous fiber sections and potential inaccuracies from the bad-channel identification step. The accuracy of the channel locations depends on the GPS spatial accuracy and the assumed fiber location. If both are obtained using commercial GPS systems, their accuracy is on average between 1 and 5 m in most encountered field environments (Wing *et al.*, 2005), which is much shorter than the commonly considered wavelengths of seismological applications (i.e., tens to thousands of meters). The overall DAS-channel mapping accuracy would decrease if an imprecise fiber map is available.

Field requirements

This section provides a few guidelines that are crucial to successfully applying our workflow when DAS data are recorded using a pre-existing dark fiber deployed by a telecommunication company. Such fibers are often deployed along existing roads, and their locations can be obtained from the owner. To geolocate all

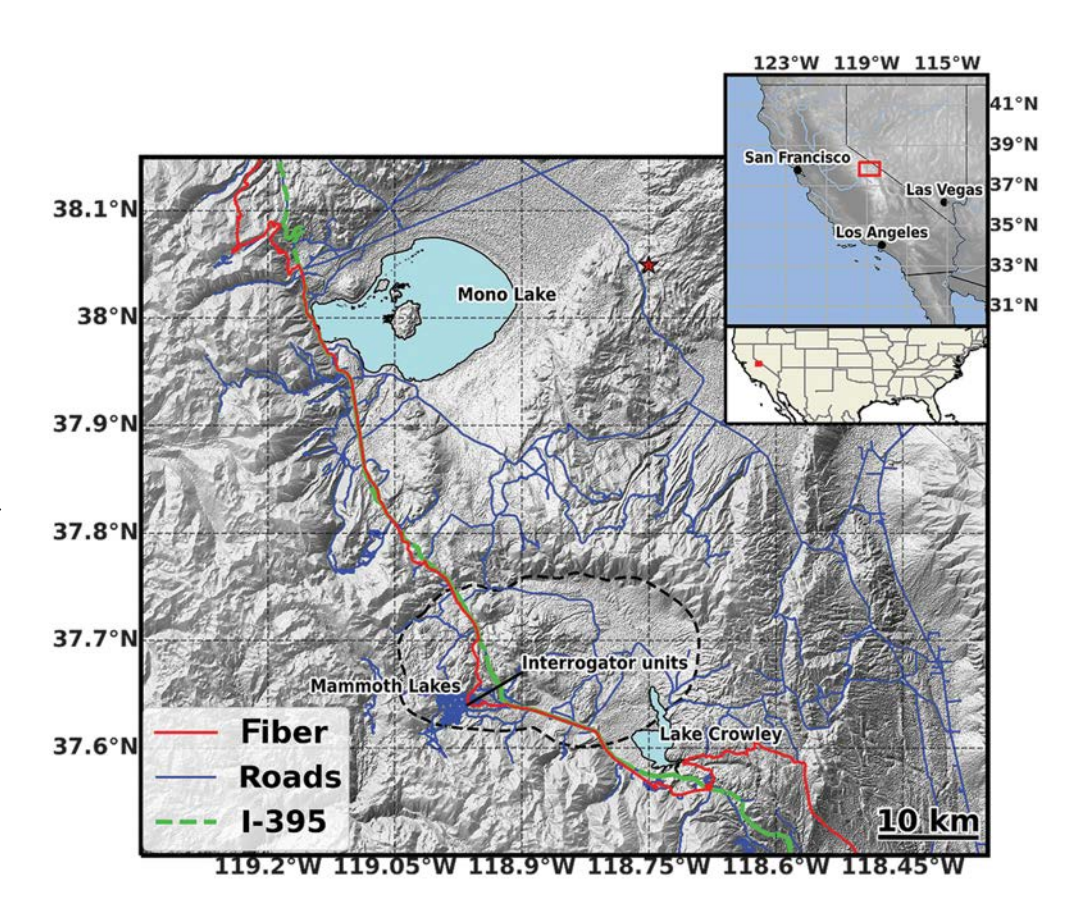
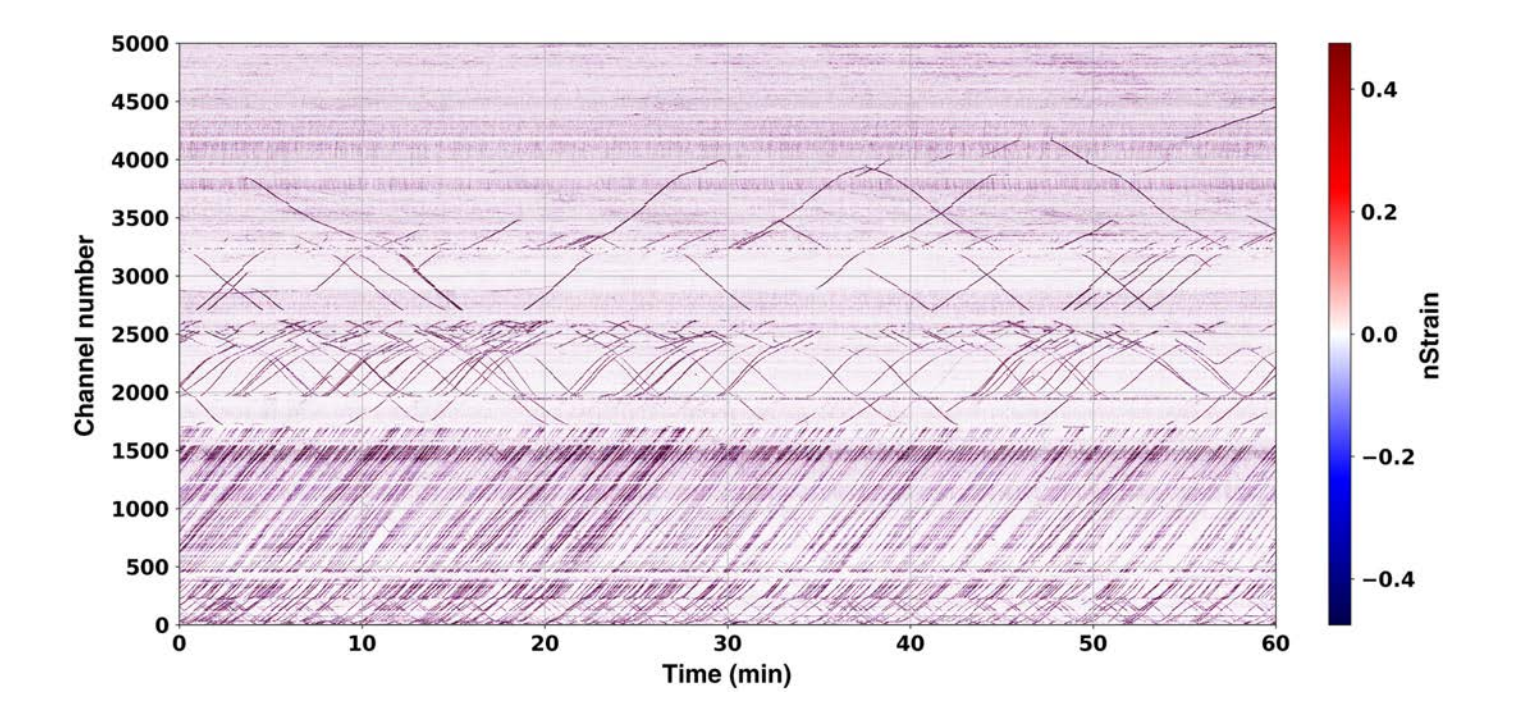


Figure 2. Location of the field application. The fiber position is depicted by the red line, whereas the blue lines depict the existing road network. The black dashed line indicates the Long Valley caldera contour. Part of the fiber is located in the proximity of the I-395 highway (green dashed line). Other sections are placed along secondary roads or dirt roads. The red star denotes the epicenter of local event considered during the calibration and verification steps. The inset in the top right corner shows the area location (red rectangle) in the United States.

channels in a DAS system, one should drive the tracked vehicle along the entire cable length sensed by the DAS.

The vehicle position as a function of time is recorded during the calibration experiment using a GPS tracker. The spatial accuracy must be below the nominal channel spacing to correctly track the vehicle within the strain records. In our case, we choose to employ a GPS tracker whose accuracy is half the channel spacing. The time sampling rate of the GPS tracker depends on the vehicle's velocity and the DAS acquisition's channel spacing, which can vary between DAS experiments. The average driving speed times the sampling rate should be lower than the channel spacing. For instance, assuming an average speed of 30 miles per hour, a vehicle covers approximately 14 m/s. Setting the GPS sampling rate to 0.5 s enables the accurate geolocalization of DAS channels with nominal spacing larger than 7 m. In our field experiment, we found that this GPS sampling rate is also suitable for higher traveling speed (e.g., 55 or 65 mile/hr general speed limit along highways), because the car position can be accurately interpolated given the usually constant vehicle's speed.



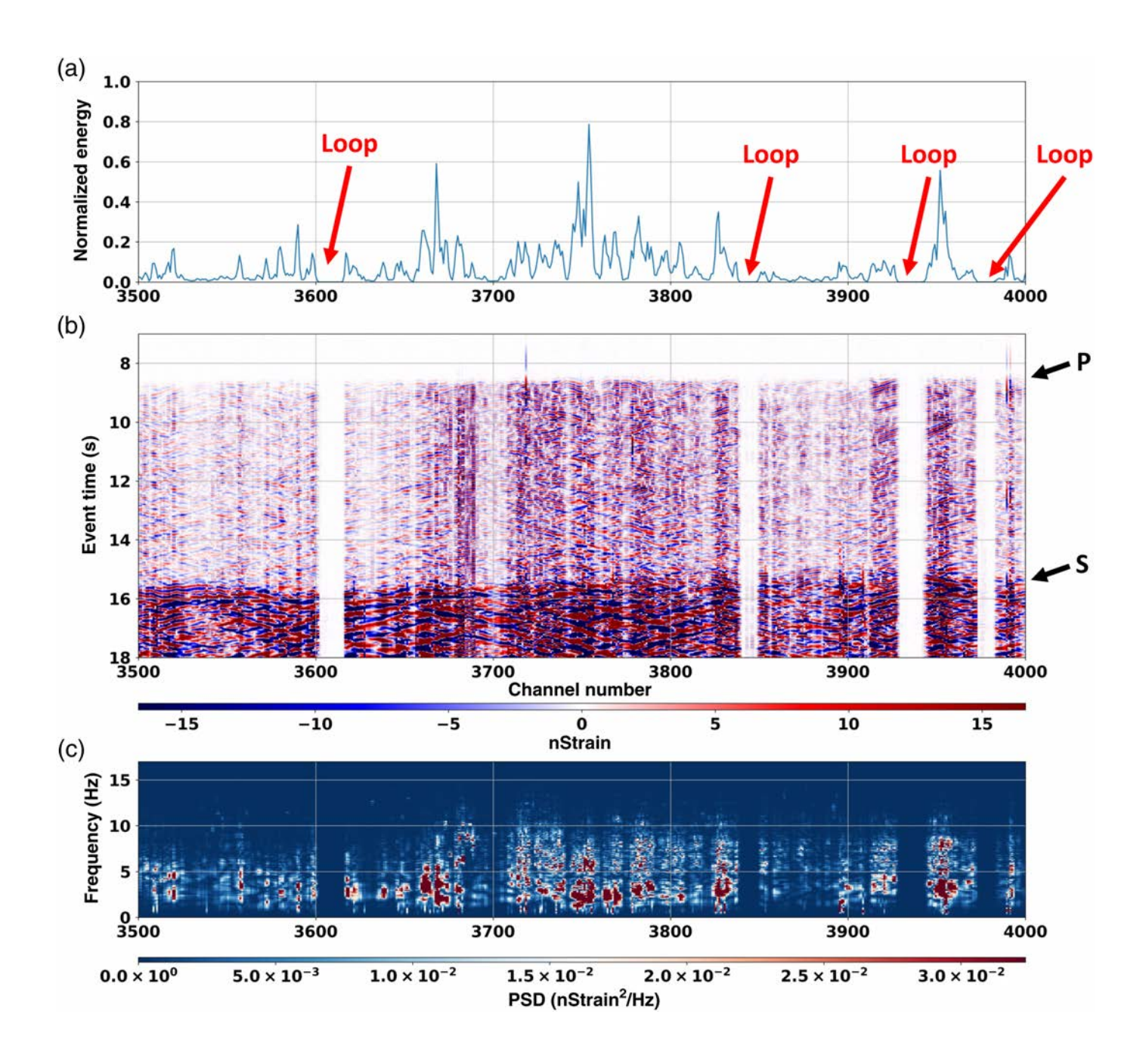
To identify the tracked vehicle within the strain records, a certain distance from other cars should be maintained whenever possible. Generally, moving vehicles generate quasi-static deformation with a dominant frequency between 0.5 and 3 Hz (Yuan et al., 2020). For this frequency band, the dominant wavelength of traffic signals is between 500 and 83 m; thus, one should maintain a distance between 20 and 125 m from other vehicles. Finally, we found that performing multiple U-turns within sections of the cable near a heavy-traffic road can simplify the identification and calibration of the tracked vehicle within the DAS recordings. Moreover, looking at the recordings before performing the calibration experiment permits determining which road lane is most effective in inducing observable quasi-static deformation. When substantial fractions of the recording fiber are positioned within hightraffic roads, this process should be applied during quiet traffic times (e.g., at night or weekends depending on the considered area).

Field Application

To show the efficacy of the proposed tap-test approach, we describe an example in which the channels of two DAS arrays covering more than 90 km of dark fiber are accurately geolocated for seismological applications. We deployed two OptaSense Plexus IUs within a telecommunication hub located in the city of Mammoth Lakes in eastern California, as shown in Figure 2. The red line in this figure depicts the geographical layout of the dark fiber used during this experiment. The fiber runs approximately northwest–southeast across the Long Valley caldera. Part of the fiber is located next to the I-395 highway, whereas other sections follow secondary roads. The fiber is encased within a high-density polyethylene conduit and

Figure 3. Hour-long data recorded by one of the two DAS systems within the Long Valley caldera showing the vehicle-induced deformation. The deformation caused by the southbound traffic along the I-395 highway is visible approximately within the first 1600 channels. The color version of this figure is available only in the electronic edition.

buried at an average depth of 1 m. One of the two DAS units interrogated the cable segment north of Mammoth Lakes, whereas the other unit interrogated the segment to the south. Both instruments were set to record data using 5000 channels with a nominal channel spacing of approximately 10 m (i.e., a combined sensing range of 100 km), and a gauge length of 20 m. The raw data sampling rates of 1000 and 2000 Hz of the two units were downsampled to 200 Hz. The seismic energy due to vehicle movements along the roads located in the vicinity of the fiber can be clearly observed on the strain records (Fig. 3). The shown data belong to the south system, and we can identify the section of the cable located along I-395 (i.e., approximately the first 1600 channels). The channels between 1600 and 3500 are located on secondary roads, whereas the last 1500 channels follow a minor quiet dirt road east of Lake Crowley. In the initial section, stronger energy is recorded from vehicles moving away from the IU, suggesting that the position of the cable is closer to the southbound lane. During the tap-test experiment, we can easily identify the tracked vehicle on the real-time data stream when driving in not high-traffic roads. This identification is crucial to the subsequent calibration step. To achieve this goal in the field, we employ a laptop computer and a smartphone mobile hotspot to remotely connect to the IU computer and monitor the data in real time.

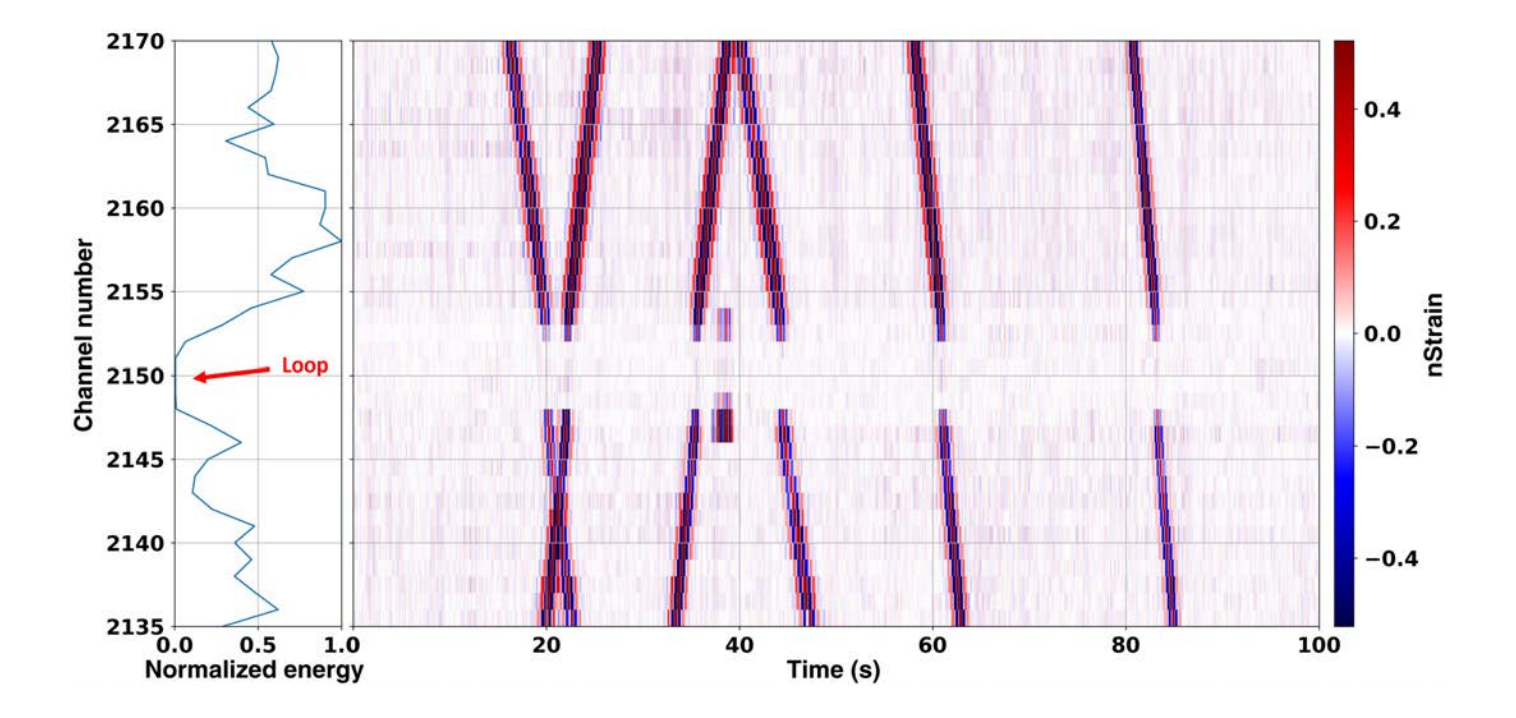


Data processing and geolocalization

We employ a local earthquake of magnitude 3.06 and depth of 8.095 km from the mean sea level (m.s.l.) recorded by the Long Valley DAS arrays to identify bad channels and fiber loops. The location of this event is depicted by the red star in Figure 2. The event ID from the double-difference catalog of the Northern California Earthquake Data Center is 73491170 (Waldhauser and Schaff, 2008), and its minimum and maximum epicentral distances from the DAS arrays are approximately 33 and 55 km, respectively. We apply a band-pass filter between 0.5 and 15 Hz to the data and remove the median of each time sample to reduce the common-mode noise usually affecting the recorded phases. The strain induced by a local earthquake on the south array highlights the channels that

Figure 4. Local earthquake recorded by a section of the south-bound fiber of the south DAS array. (a) The normalized energy of the signal recorded by each channel. The red arrows indicate the location of fiber loops. (b) The strain as a function of the event's origin time and the *P*- and *S*-wave arrival are marked on the side. (c) The power spectral density (PSD) of each channel computed using the 11 s data window of panel (b). The color version of this figure is available only in the electronic edition.

are part of a fiber loop (Fig. 4). The limited coupling of the fiber in these sections also affects their energy content and the power spectral density (PSD) at different frequencies. These channels are selected and discarded from the calibration analysis. This identification process starts using equation (1)



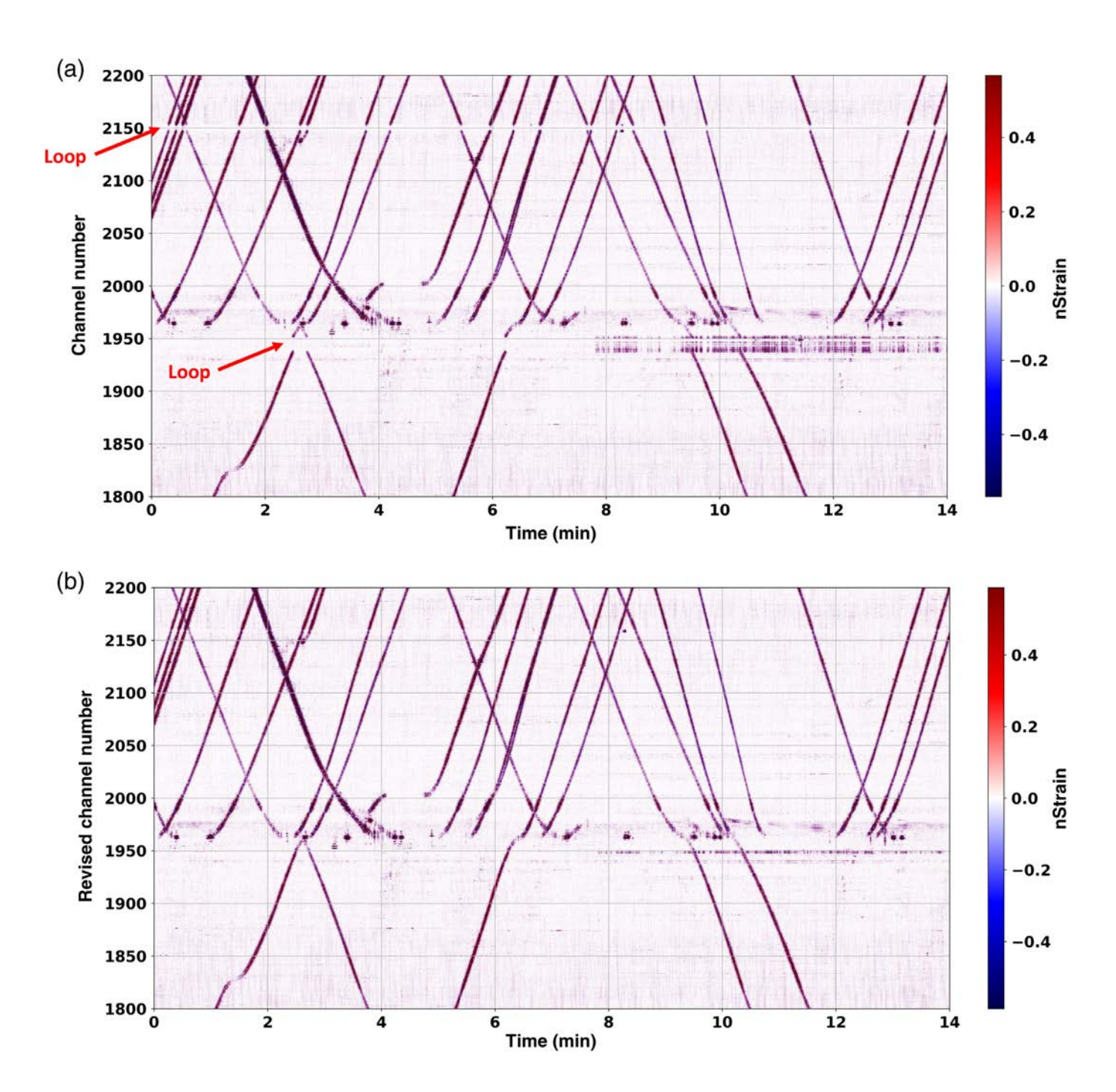
and is then verified and refined using an interactive plotting tool. Local and regional earthquakes provide the best signal to perform this identification task, which on each section act as plane waves impinging on a fiber (Lindsey, Rademacher, and Ajo-Franklin, 2020), but traffic energy or the quasi-static deformation of the tracked vehicle can also be employed for this purpose (Fig. 5). Figure 6 shows the recorded strain on a section of the south cable in which traffic noise is displayed before and after removing the channels associated with fiber loops. Once the fiber loops are removed, the vehicle signals present a more coherent and continuous moveout within the data panel.

The next step is the calibration of the vehicle distance–time curve with the corresponding quasi-static deformation. In this step, the car's along-fiber distance can be shifted by an arbitrary positive and negative value along the channel axis. This shifting allows us to match the car-generated signal with the actual car position at a given time. The points where the vehicle-generated seismic energy overlaps with the distance curve imply that the position of the vehicle was near a recording channel (Fig. 7c). Thus, the car position can be used to locate a given DAS channel, just like any controlled-source experiment. The ability to clearly identify this geo-tracked quasi-static deformation within the data depends on the relative car-fiber distance. When the vehicle is within 20 m from the fiber, this signal is clearly visible. In our case, the average car-fiber distance within the geotracked sections is 7 m. However, if this distance is greater, then no clear signal is recorded. For instance, this behavior can be seen within the recordings between 60 and 80 s in Figure 7. The channels within these sections are interpolated using either the provided fiber location or the car positions depending on which one is

Figure 5. Recorded strains and corresponding channel energy for an approximately 500 m section of the southbound fiber highlighting the small amplitudes present within a fiber loop. The color version of this figure is available only in the electronic edition.

assumed to be more accurate. Overall, this process permits to locate multiple channels quickly. In this step, quiet roads and U-turns can be used to easily identify the tap-test vehicle within the data panels (Fig. 8a). For instance, Figure 8b shows how the signal recorded on a secondary road is used to track the vehicle within a busy highway. Moreover, U-turns result in unique curve patterns that are easily recognizable (Fig. 8c). By performing this process for the entire cable length, we obtain the position of most of the DAS channels. The unusually short sections in which a clear vehicle signal could not be identified are obtained by a linear interpolation process using the edge channel positions. The final step is to remap the identified channel positions onto the corresponding closest fiber cable points. A final verification is performed by mapping the vehicle positions onto the closest channels as function of time. Figure 9 shows an example of this verification step for the south array. The GPS position is transformed into the closest DAS channel as a function of time (green dashed line), which is then overlaid to the recorded strain data. In this example, we show that we track the vehicle along more than 30 km of cable.

Figure 10 displays the channel locations with every 1000th channel marked. The instruments are located in the proximity of the zeroth channels, which are inside the Mammoth Lakes telecommunication hub. The last north-system channel reaches Mono Lake, whereas the south-system crosses the Lake

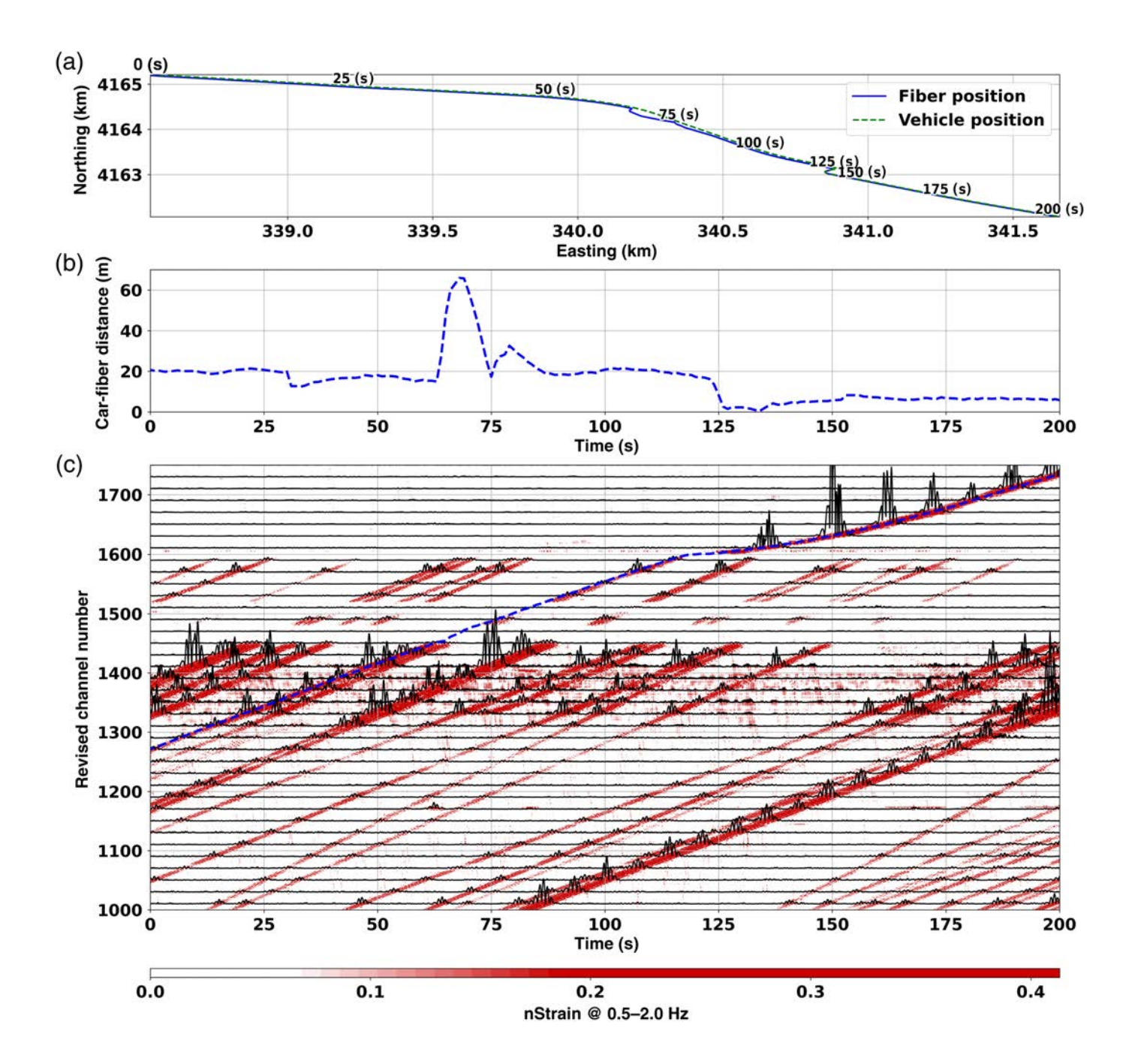


Crowley dam and ends in an uninhabited region. The approximately 9000 useful channels of the two DAS arrays cover more than 90 km with approximately regular spacing of 10 m (see close-up in Fig. 10). The mean channel spacing is 10.1 m with a standard deviation of 1 m, which is close to the set optical channel distance of 10.2 m.

The combination of two DAS IUs permits recording of local, regional, and teleseismic events with a large-scale and dense linear array. As an example of such recordings, Figure 11 displays the strain induced by the same local event of Figure 4 in which P- and S-wave arrivals are clearly distinguishable. By calibrating the channel positions and removing the fiber loops, we produce laterally continuous waveform data plotted using the correct channel

Figure 6. Recorded deformations along a section of the cable (a) before and (b) after removing bad channels and fiber loops. The red arrows indicate the fiber loops causing the gaps in recorded vehicle signals. The color version of this figure is available only in the electronic edition.

distance covered by the fiber (Fig. 12). Moreover, scattered surface waves generated by the P arrival are also visible between 10 and 35 km. The described process enables the possibility of rapid deployment and calibration of DAS systems to record postseismic processes after major earthquakes, which is critical to characterize the seismicity of an active fault (Li et al., 2021).



Conclusions

We present a novel and efficient methodology to map channels of a DAS system recording strain data using telecommunication dark fibers. Our workflow relies on a GPS-tracked vehicle moving in the proximity of the sensing cable. This approach can be applied whenever paved or unpaved roads are close to the detecting fiber. We describe the necessary steps composing our procedure and discuss the field requirements to apply it. We show how uninformative channels can be identified and removed from any further data analysis and how the geolocalization process is performed using the quasi-static deformation induced by the GPS-tracked vehicle. Our procedure greatly diminishes the fieldwork time compared to point-wise methodologies and enables the prompt deployment

Figure 7. Vehicle-fiber distance and signal tracking plots. (a) The known fiber location (blue solid line) and the global positioning system (GPS)-tracked vehicle position (green dashed line) plotted along with relative time marks used within the three panels. This marks highlight that the vehicle is moving from northwest toward southeast. (b) The car-fiber distance as function of time. (c) The GPS-tracked-vehicle-distance curve (blue dashed line) on top of the envelope of the recorded strain. In this panel, the black traces are the strain envelope for every 20 channels. The color version of this figure is available only in the electronic edition.

of DAS units to monitor aftershocks of large earthquakes or to assess any other seismological phenomenon related to geo-hazards.

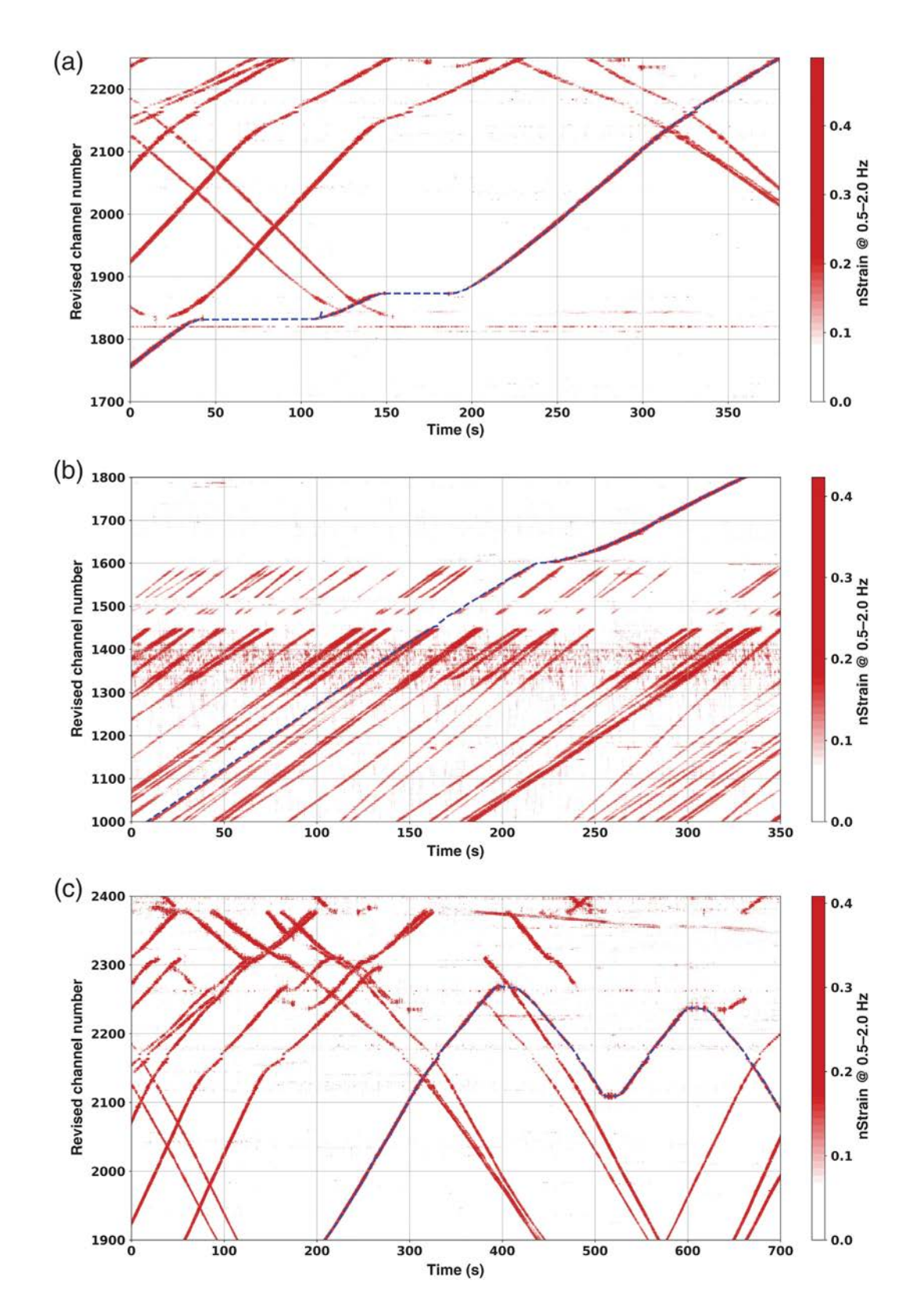
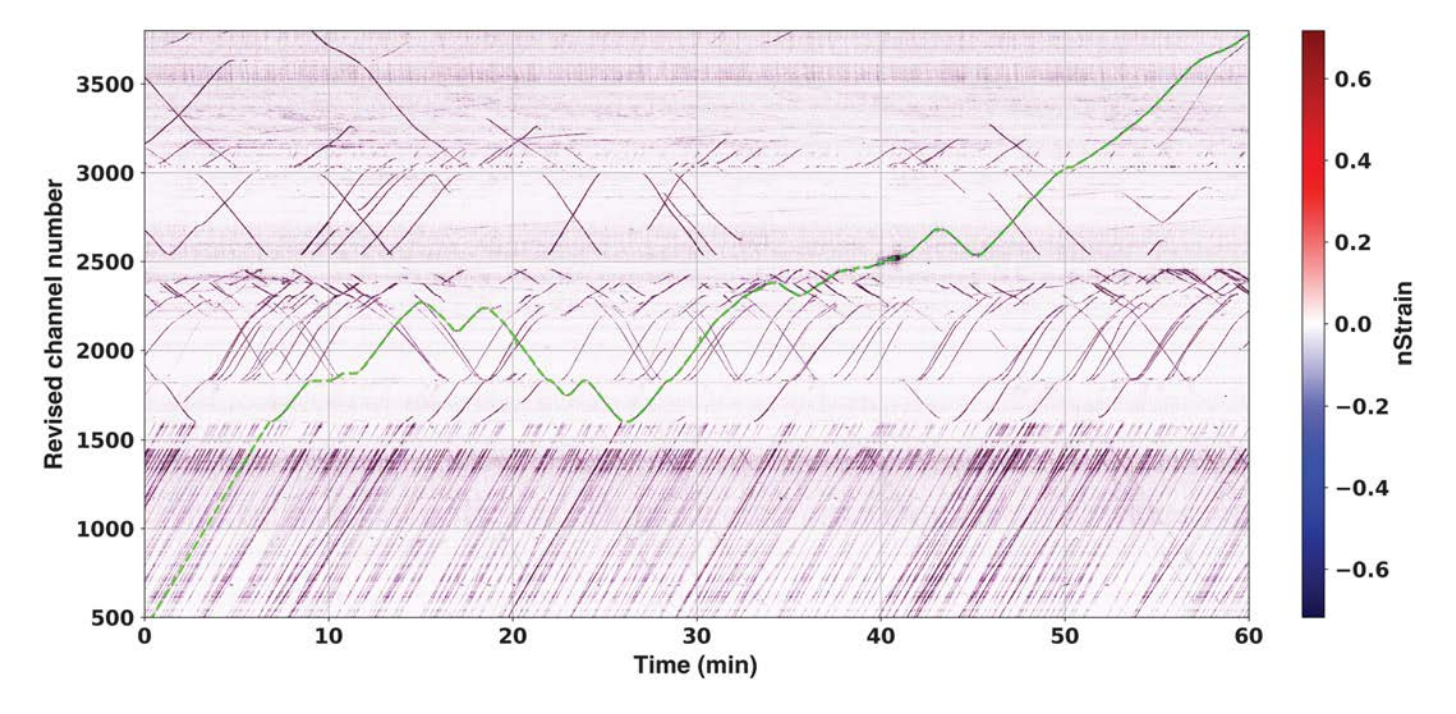


Figure 8. GPS-tracked-vehicle-distance curve (blue dashed line) alignment with the recorded DAS data within (a) a quiet road and when the car stopped at two traffic stops, (b) a highway section

followed by a secondary road, and (c) when performing three U-turns.



Data and Resources

The source code used to calibrate the described two systems can be found in the GitHub repository (https://github.com/biondiettore/DAS-taptest-widgets.git, last accessed August 2022). In addition to the interactive Python widgets, the reader can find a tutorial guiding

a user throughout the entire localization procedure (i.e., from bad channel identification to calibration step). The tutorial allows the reader to download the data part of this work. The supplemental figure S1 shows the same local event as in Figures 11 and 12 in which the channels are sorted by the epicentral distance computed using inaccurate interpolated channel positions and the calibrated locations.

Declaration of Competing Interests

The authors acknowledge that there are no conflicts of interest recorded.

Acknowledgments

The authors would like to thank OptaSense for the support provided for this calibration experiment. In particular, the authors thank Martin Karrenbach, Victor Yartsev, and Vlad Bogdanov. The authors also thank the California Broadband Cooperative for

Figure 9. Verification of the final channel positions using the recorded DAS data during the tap-test along the south array. The green dashed line displays the closest channel for each position of the GPS-tracked vehicle as function of time.

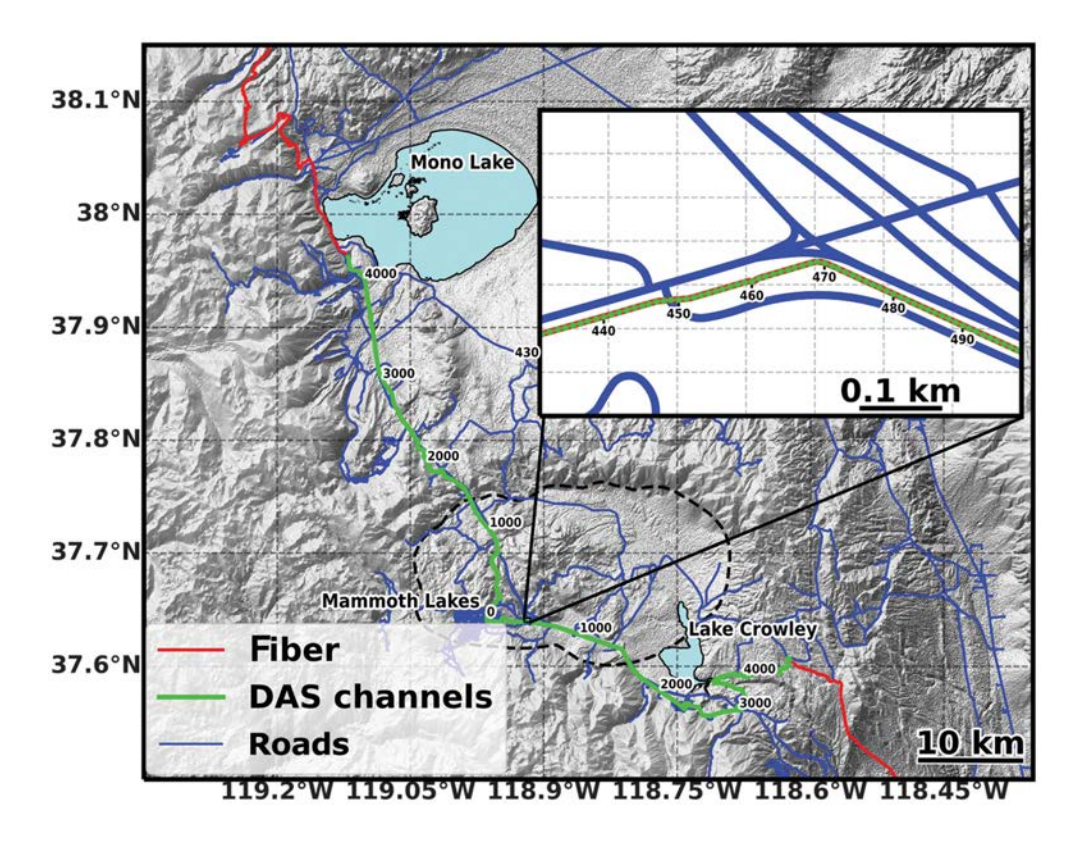
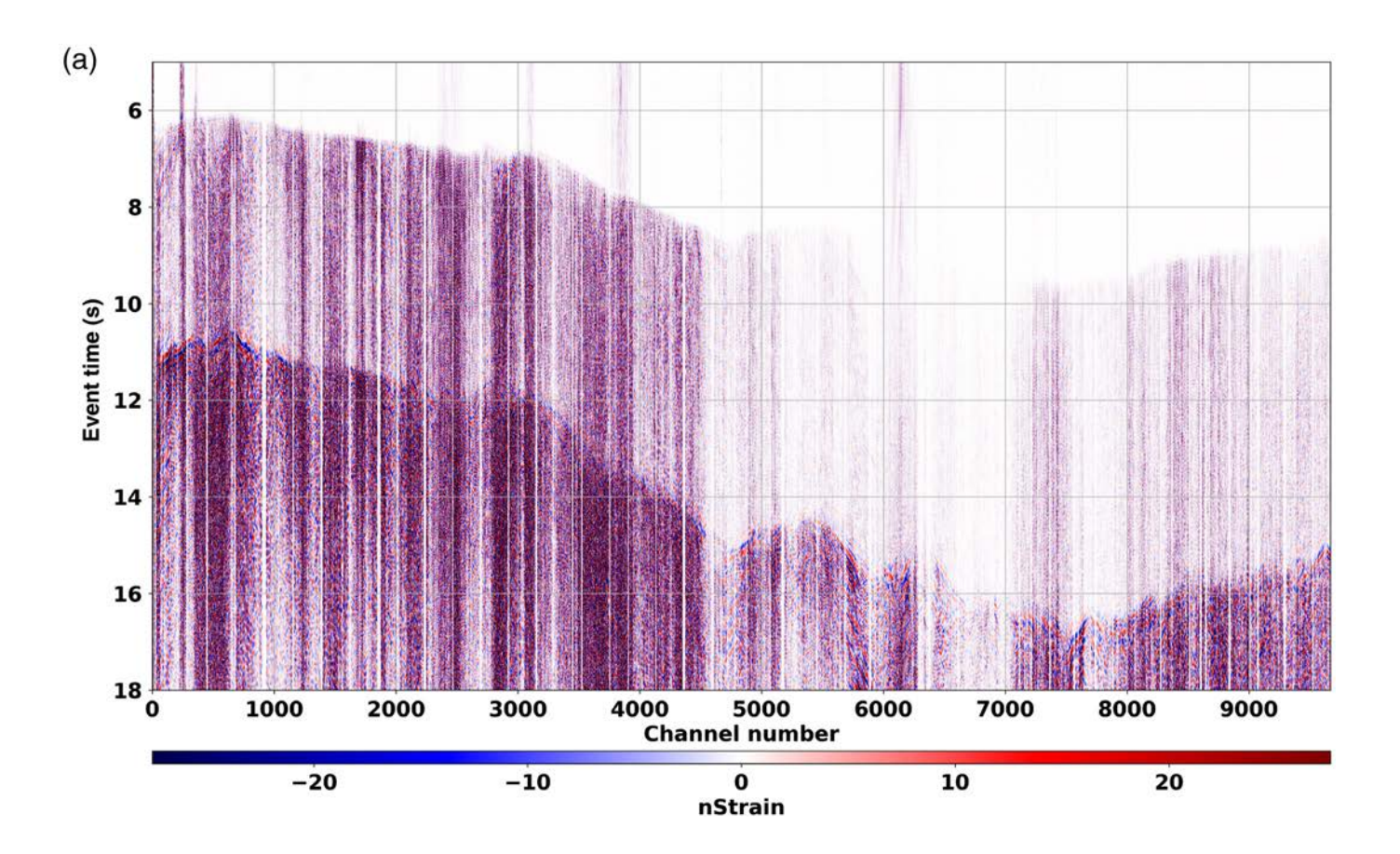


Figure 10. Final channel positions of the two DAS systems. The overall distance covered by the useful channels is approximately 90 km. The red, green, and blue curves indicate the fiber, DAS channel, and road map locations, respectively. In the inset, the same color scheme is used to indicate the displayed variables.



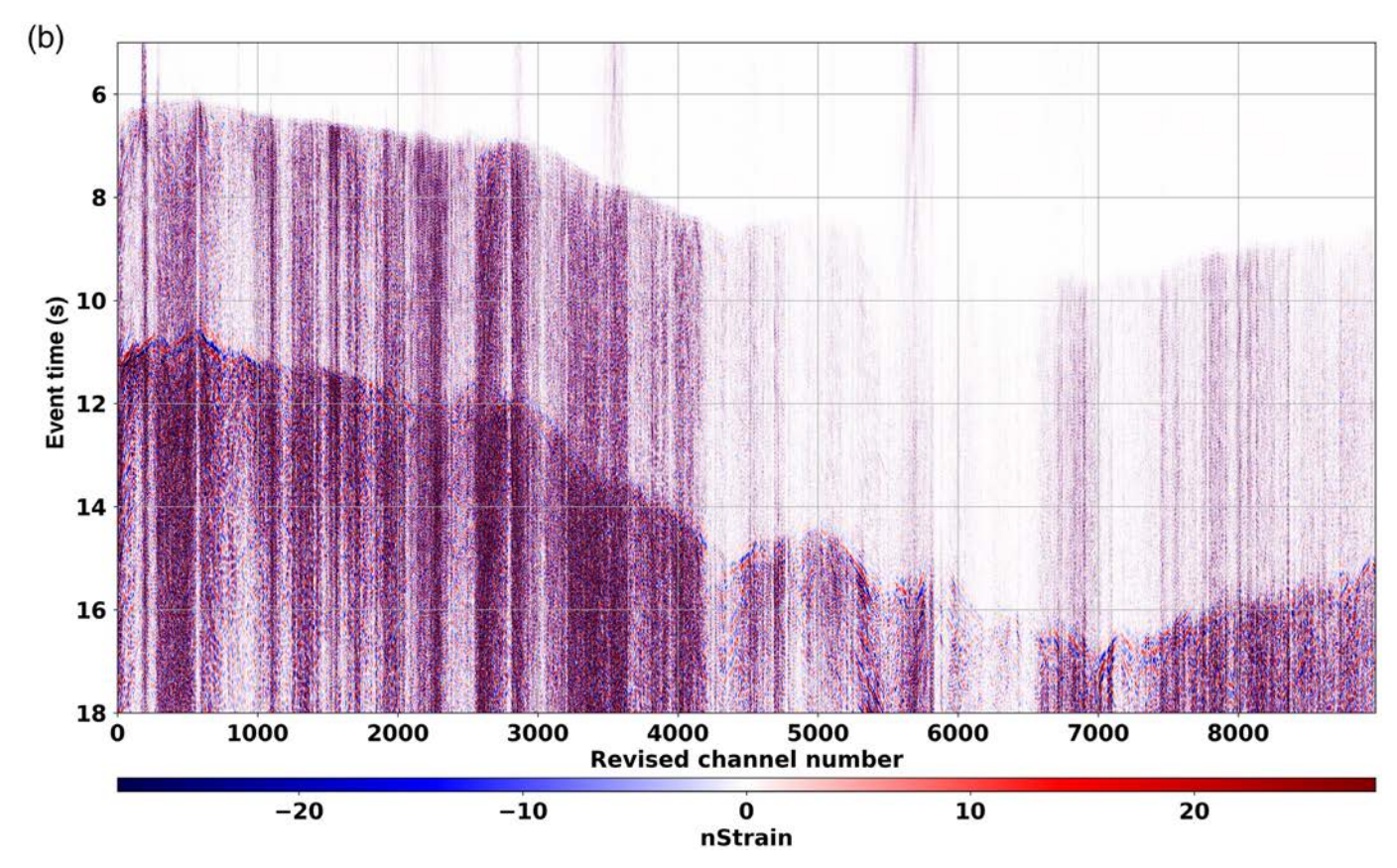
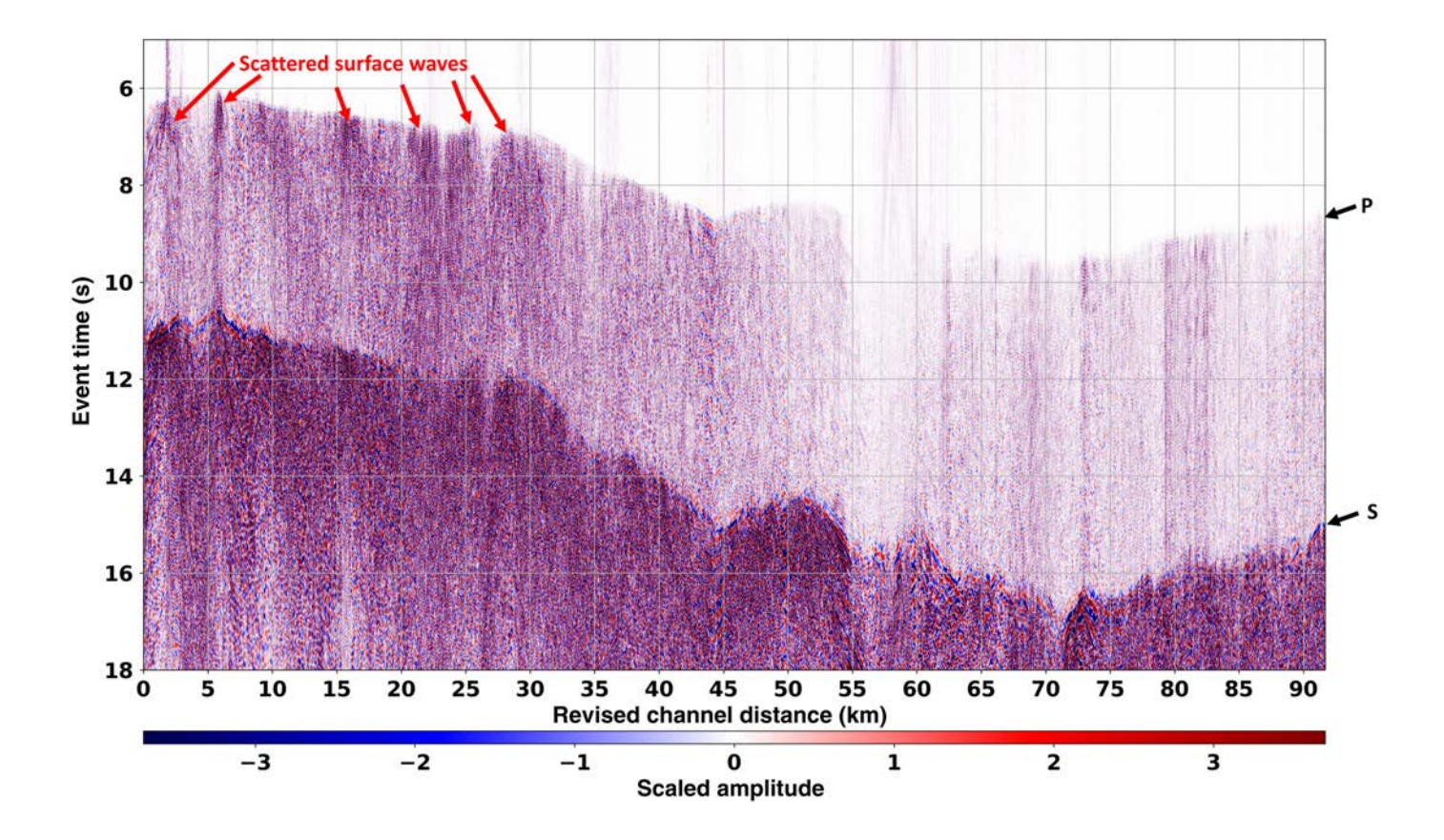


Figure 11. Local event of magnitude 3.06 recorded by both systems. Strain records (a) before and (b) after the calibration process. Because all channels belonging to fiber loops are removed the

bottom panel presents a more contiguous amplitude variation across the channel axis. The color version of this figure is available only in the electronic edition.

www.srl-online.org • Volume 94 • Number 1 • January 2023



providing access to the Digital 395 telecommunication fibers. The authors also thank James Atterholt and Jiaxuan Li for their insightful suggestions. Finally, the authors would like to thank Ariel Lellouch and two anonymous reviewers for their careful reading of their article and their many constructive comments and suggestions. This work is supported by National Science Foundation (NSF) Faculty Early Career Development Program (CAREER) Award Number 1848166, the Resnick Institute of Sustainability, and the Gordon and Betty Moore Foundation.

References

Ajo-Franklin, J. B., S. Dou, N. J. Lindsey, I. Monga, C. Tracy, M. Robertson, and T. Daley (2019). Distributed acoustic sensing using dark fiber for near-surface characterization and broadband seismic event detection, Sci. Rep. 9, no. 1, 1–14.

Biondi, B. L., S. Yuan, E. R. Martin, F. Huot, and R. G. Clapp (2021). Using Telecommunication fiber infrastructure for earth-quake monitoring and near-surface characterization, in *Distributed Acoustic Sensing in Geophysics: Methods and Applications*, Y. Li, M. Karrenbach, and J. B. Ajo-Franklin (Editors), John Wiley & Sons, Inc., Hoboken, New Jersey, 131–148.

Huot, F., E. R. Martin, and B. Biondi (2018). Automated ambient noise processing applied to fiber optic seismic acquisition (DAS), SEG Technical Program Expanded Abstracts 2018, Society of Exploration Geophysicists, 4688–4692.

Karrenbach, M., V. Yartsev, S. Cole, and R. Hooper (2021). Long-range seismicity monitoring with DAS, First International Meeting for Applied Geoscience & Energy, 1216–1220.

Figure 12. Interpretation of the panel in Figure 11b. In this plot, each channel is normalized by its standard deviation. The red arrows indicate locations in which scattered surface waves are excited by the impinging earthquake, whereas the black arrows indicate the *P*- and *S*-wave arrivals. The color version of this figure is available only in the electronic edition.

Klaasen, S. A., P. Paitz, N. Lindner, J. Dettmer, and A. Fichtner (2021). Distributed acoustic sensing in volcano-glacial environments-Mount Meager, British Columbia, J. Geophys. Res. 126, no. 11, doi: 10.3929/ethz-b-000518921.

Li, Z., Z. Shen, Y. Yang, E. Williams, X. Wang, and Z. Zhan (2021). Rapid response to the 2019 Ridgecrest earthquake with distributed acoustic sensing, AGU Adv. 2, no. 2, e2021AV000395, doi: 10.1029/2021AV000395.

Lindsey, N. J., T. C. Dawe, and J. B. Ajo-Franklin (2019). Illuminating seafloor faults and ocean dynamics with dark fiber distributed acoustic sensing, *Science* 366, no. 6469, 1103–1107.

Lindsey, N. J., S. Yuan, A. Lellouch, L. Gualtieri, T. Lecocq, and B. Biondi (2020). City-scale dark fiber DAS measurements of infrastructure use during the COVID-19 pandemic, *Geophys. Res. Lett.* 47, no. 16, e2020GL089931, doi: 10.1029/2020GL089931.

Lindsey, N. J., H. Rademacher, and J. B. Ajo-Franklin (2020). On the broadband instrument response of fiber-optic DAS arrays, J. Geophys. Res. 125, no. 2, e2019JB018145, doi: 10.1029/ 2019JB018145.

Liu, H., J. Ma, W. Yan, W. Liu, X. Zhang, and C. Li (2018). Traffic flow detection using distributed fiber optic acoustic sensing, *IEEE Access* **6**, 68,968–68,980.

- Martin, E., and B. Biondi (2018). Eighteen months of continuous near-surface monitoring with DAS data collected under Stanford University, SEG Technical Program Expanded Abstracts 2018, Society of Exploration Geophysicists, 4958–4962.
- Martin, E., B. Biondi, M. Karrenbach, and S. Cole (2017). Continuous subsurface monitoring by passive seismic with distributed acoustic sensors the "Stanford Array" experiment, *First EAGE Workshop on Practical Reservoir Monitoring*, cp–505.
- Nayak, A., J. Ajo-Franklin, and , and I. V. D. F. Team (2021). Distributed acoustic sensing using dark fiber for array detection of regional earthquakes, Seismol. Soc. Am. 92, no. 4, 2441–2452.
- Tribaldos, V. R., J. B. Ajo-Franklin, S. Dou, N. J. Lindsey, C. Ulrich, M. Robertson, and C. Tracy (2021). Surface wave imaging using distributed acoustic sensing deployed on dark fiber: Moving beyond high-frequency noise, in *Distributed Acoustic Sensing in Geophysics: Methods and Applications*, Y. Li, M. Karrenbach, and J. B. Ajo-Franklin (Editors), John Wiley & Sons, Inc., Hoboken, New Jersey, 197–212.
- Waldhauser, F., and D. Schaff (2008). Large-scale cross correlation based relocation of two decades of northern California seismicity, *J. Geophys. Res.* **113**, no. B8, doi: 10.1029/2007JB005479.
- Wang, X., E. F. Williams, M. Karrenbach, M. G. Herráez, H. F. Martins, and Z. Zhan (2020). Rose Parade seismology:

- Signatures of floats and bands on optical fiber, Seismol. Res. Lett. 91, no. 4, 2395–2398.
- Wing, M. G., A. Eklund, and L. D. Kellogg (2005). Consumer-grade global positioning system (GPS) accuracy and reliability, *J. For.* 103, no. 4, 169–173.
- Yang, Y., J. W. Atterholt, Z. Shen, J. B. Muir, E. F. Williams, and Z. Zhan (2022). Sub-kilometer correlation between near-surface structure and ground motion measured with distributed acoustic sensing, *Geophys. Res. Lett.* 49, no. 1, e2021GL096503, doi: 10.1029/2021GL096503.
- Yuan, S., A. Lellouch, R. G. Clapp, and B. Biondi (2020). Near-surface characterization using a roadside distributed acoustic sensing array, *The Leading Edge* **39**, no. 9, 646–653.
- Yuan, S., J. Liu, H. Young Noh, and B. Biondi (2021). Urban system monitoring using combined vehicle onboard sensing and roadside distributed acoustic sensing, First International Meeting for Applied Geoscience and Energy, Denver, Colorado.
- Zhan, Z. (2020). Distributed acoustic sensing turns fiber-optic cables into sensitive seismic antennas, *Seismol. Res. Lett.* **91**, no. 1, 1–15.

Manuscript received 23 May 2022 Published online 15 September 2022